Holdup and Interfacial Area Measurements Using Dynamic Gas Disengagement

The dynamic gas disengagement technique is discussed comprehensively in this paper. Also outlined is the procedure for estimating holdup structures and bubble rise velocities in a bubble column, which is extended to include the methodology for estimating the Sauter mean bubble diameter and therefore the specific gas-liquid interfacial area. The error limits for the estimated quantities are established using two extreme cases to describe the disengagement process: constant rate disengagement and interactive disengagement of bubbles. The analysis is done assuming a bimodal bubble size distribution; however, generalized equations for a multimodal bubble size distribution are also presented. Sensitivity of results to the two cases is illustrated using results obtained from experiments conducted with the air-tap water system in two bubble columns (0.05 and 0.23 m in diameter, 3 m tall). Sauter mean bubble diameters and specific interfacial areas estimated using the two approaches provide lower and upper limits for values reported in the literature.

Snehal A. Patel
James G. Daly
Dragomir B. Bukur
Kinetics, Catalysis and Reaction Engineering Laboratory
Department of Chemical Engineering
Texas A&M University
College Station, TX 77843

Introduction

A precise knowledge of the gas holdup structure and bubble size distribution is essential for evaluating the performance of bubble column reactors, and the dynamic gas disengagement (DGD) technique is increasingly being used to study the hydrodynamics of such reactors. The technique, first introduced by Sriram and Mann (1977), requires an accurate measurement of the rate at which the level of the gas-liquid dispersion drops once gas flow to the bubble column is shut off. The measured disengagement profile is then used to estimate the holdup structure that existed in the dispersion prior to flow interruption. The bubble size distribution, and therefore the gas-liquid interfacial area, can also be determined using appropriate correlations that relate bubble sizes to bubble rise velocities.

Sriram and Mann presented the theoretical basis for this technique and showed that the static and dynamic disengagement holdups are dictated by the size distributions and the rise velocity functions of the bubbles. They assumed that the dispersion, prior to flow interruption, was axially homogeneous, and there was no bubble-bubble interaction once gas flow was cut off: i.e., the identity of the individual bubbles was preserved. However, their work with the air-water system was limited to low gas holdups (<5%); and for this range of holdups, they showed that some ambiguity is inherent in the technique when predicting bubble size distributions. This is because, for identical disengagement profiles, different bubble size distributions would be obtained if different liquid circulation intensities are assumed, and an independent measurement of one property would be necessary to accurately estimate the other. When they neglected liquid circulation, they showed that a log-normal bubble size distribution described the disengagement profile very well.

The approach presented by Sriram and Mann has been used by several researchers to determine the holdup structure of the dispersion. In most cases, the dispersion was assumed to consist of one or two dominant bubble sizes. Vermeer and Krishna (1981) applied this approach to the nitrogen-turpentine 5 system. They assumed a bimodal distribution with large bubbles forming the transport portion of the holdup and small slow-moving bubbles forming the entrained portion. Based on this assumption, they considered the initial part of the disengagement profile to be dictated solely by the large bubbles, with the small bubbles disengaging only after all of the large bubbles have left the system. They used the resulting disengagement profiles to estimate the contribution to gas holdup by the two

Correspondence concerning this paper should be addressed to D. B. Bukur.

bubble classes. Schumpe and Deckwer (1982), and Godbole et al. (1982, 1984) conducted experiments with highly coalescing CMC (carboxymethyl cellulose) systems and used bimodal bubble size distributions to determine the holdup structure of the dispersion by dynamic gas disengagement. For such systems, they have shown that the contribution of small bubbles to the overall gas holdup is negligible. In similar experiments with different concentrations of surfactants added to the CMC solution, Godbole et al. (1984) showed that the contribution of small bubbles to the overall gas holdup increased with increasing surfactant concentration (i.e., decreasing coalescence rates), while the contribution due to large bubbles remained virtually unchanged. In experiments conducted with alcohol solutions (noncoalescing media) by Kelkar et al. (1983), similar results were obtained when the holdup structure was determined using the dynamic gas disengagement technique assuming a bimodal bubble size distribution. For these solutions, the contribution to overall gas holdup by small bubbles was even greater than that due to large bubbles.

More recently, Schumpe and Grund (1986) have presented results for the air-water system, with an emphasis on some of the problems associated with the DGD technique and have proposed corrective measures that to some extent can alleviate these problems. The problems analyzed by the authors include the subjectivity involved in obtaining an accurate disengagement profile during large bubble disengagement, the "waterfall" effect or the downward flow of liquid during bubble disengagement and its impact on the rise velocities of small bubbles that are still in the system, and the errors introduced by bubbles entering the dispersion as the pressure in the plenum chamber equilibriates with the hydrostatic pressure of the dispersion, following the interruption of the gas supply. The authors assumed a bimodal bubble size distribution in their analysis and presented the gas holdup structure as well as bubble rise velocities for the two bubble classes. The problems associated with obtaining accurate disengagement profiles were also discussed by Lee et al. (1985), who developed a digital sensor with a computer interface that greatly improved accuracy and reproducibility of the measured disengagement profile.

In the studies discussed above, the disengagement profiles were plotted as either dynamic gas holdup vs. time (e.g., Schumpe and Deckwer, 1982; Godbole et al., 1982, 1984; Lee et al., 1985) or as dispersion height vs. time (e.g., Vermeer and Krishna, 1981; Schumpe and Grund, 1986). In each case, the profile was described by two straight lines, representing the two phases of bubble disengagement. The first phase involves the disengagement of all of the large bubbles and some of the small bubbles (or no small bubbles), and the second phase represents the disengagement of small bubbles alone. The fitting of straight lines to the dynamic gas holdup profiles involves a major approximation of the original equation proposed by Sriram and Mann (1977). The assumption is that the change in height of the dispersion (H_o-H_s) is sufficiently small relative to the static height (H_s), which is true only for very low gas holdups. This point is further elaborated later in the paper.

Researchers at Mobil (Kuo, 1985) were the first to discretize Sriram and Mann's original equation without introducing any new assumptions other than a noncontinuous distribution. They applied the resulting equations to disengagement profiles obtained from experiments using molten wax as the liquid medium at low gas velocities and assumed unimodal or bimodal bubble size distributions. The quantities estimated in their study included the gas holdup structure, bubble rise velocities, and bubble sizes.

It is our intention to present a comprehensive discussion of the DGD theory in an effort to put into proper perspective some of the discrepancies among different approaches, and to show how information obtained from DGD can be used to determine Sauter mean bubble diameters. A discretized set of generalized equations are developed to describe a system with a multimodal bubble size distribution, and the procedure to estimate bubble diameters and Sauter mean bubble diameters is also presented. Results from experiments with the air-tap water system are used to illustrate the theory.

Experimental Technique

Dynamic gas disengagement measurements were carried out in two glass columns (0.05 and 0.23 m diameter, 3 m tall). A 2 mm orifice plate distributor was used in the small (0.05 m ID) column, and a 19 × 2 mm perforated plate distributor was used in the large (0.23 m ID) column. All experiments were conducted under ambient conditions. A videocamera and a VCR unit were used to record the drop in liquid level during the disengagement process. A vertical ruler mounted next to the column (in the camera's field of view) was used to obtain the actual heights. After achieving steady state at a given gas velocity, the gas flow to the column was shut off using a solenoid valve and the drop in liquid level recorded. Initially, the level dropped rapidly due to the disengagement of large bubbles. Thereafter, the level dropped slowly as smaller bubbles disengaged from the dispersion. The recording was completed when the level reached a stationary value (corresponding to the static height).

The data reduction procedure involved the analysis of the video tape followed by the parameter estimation step. The video tape was scanned, and the time elapsed was recorded for different values of height as the level dropped during the disengagement process. The scanning procedure was repeated three to four times for each velocity to minimize errors. The data were recorded directly into a personal computer. The frequency, at which time was recorded, ranged from every 0.05 m drop in level (during the first phase when the level dropped rapidly) to every 0.005 m drop in level towards the end when smaller bubbles were disengaging. Following this step, the normalized liquid level (H/H_o) vs. time plot was displayed directly on the screen. The break point in the curve was then identified, and the data were fitted with two straight lines. The slopes and intercepts of the straight line segments were then computed and the corresponding rise velocities, holdup fractions, bubble diameters, etc., estimated.

A major drawback of using the above procedure for measuring the disengagement profile is the uncertainty involved in obtaining data during the first phase (large bubble disengagement). During this period, the liquid surface is not defined clearly because of the splashing caused by large bubbles leaving the dispersion. We were able to reduce the errors to some extent by scanning the video tape several times and averaging the data. However, this process is time-consuming and tedious. Various alternatives have been suggested in the literature for measurement of the disengagement profiles. Schumpe and Grund (1986) have suggested that the problem associated with large bubble disengagement can be avoided by estimating the profile during this period instead of measuring it. Lee et al. (1985) have

attempted to better define the liquid surface by using a wooden buoy, interfaced to a digital sensor that floats on the surface and is not significantly affected by liquid splashing. Weimer et al. (1985) used a gamma-radiation density gauge to obtain the height of a fluidized bed as a funciton of time once gas flow was cut off. The latter technique does not require any visual observations and can be employed to study hydrodynamics of systems at high temperatures and/or high pressures.

Theory

In the following analysis, we shall assume that the dispersion is axially homogeneous at the instant when gas flow is interrupted and there are no bubble-bubble interactions. These assumptions are the same as those used by Sriram and Mann (1977), and they approximate the true hydrodynamics of the dispersion. Deviations from these assumptions may occur in strongly coalescing systems at high gas flow rates, particularly in the region immediately above the distributor. Disengagement profiles measured in most studies indicate the presence of two dominant bubble-size classes. We have, therefore, used a bimodal bubble size distribution in our analysis. However, we have also shown how the theory can be extended to the case of a multimodal bubble size distribution.

The dispersion volume for the bimodal case can be partitioned into three fractions representing the liquid volume, total volume of large bubbles, and the total volume of small bubbles, respectively. Under the assumption of axial homogeneity, the dispersion, just before the gas flow is cut off, can be represented by Figure 1. The volumes of the three components are proportional to the respective holdup fractions. The disengagement process can be envisioned as either a constant rate process, where the small and large bubbles disengage independent of one another (case I), or as an interactive process, where the disengagement of large bubbles retards the disengagement rate of small bubbles (case II). Even though the latter case is interactive, it does not account for bubble-bubble interaction. A third, although less likely, possibility is the case where the disengagement of large bubbles enhances the disengagement rate of small bubbles. This could happen if the small bubbles adhere to the large bubble surface and disengage along with them. The actual disengagement process is expected to lie between the two extremes described by cases I and II.

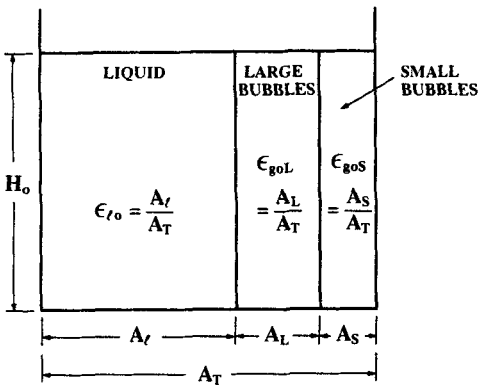

Figure 1. Dispersion at the beginning of the disengagement process ($t = 0$).

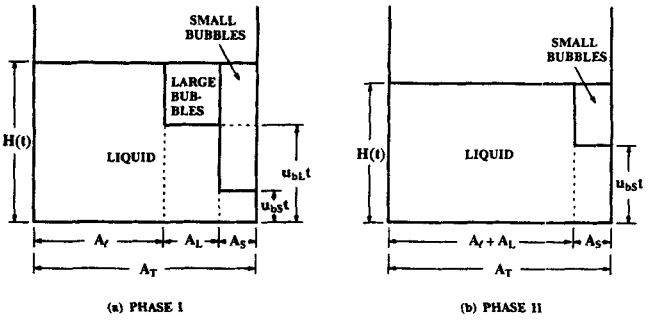

Figure 2. Dispersion during the constant rate disengagement process.

Case I: constant rate disengagement process

Before analyzing this case, it is important to define the constant rate disengagement process. Under these conditions, the volumes representing the small and large bubbles (Figure 1) move away form the bottom of the column (disengage) at constant rise velocities. Furthermore, if we assume each volume to be a column of gas with a constant cross-sectional area, then this constancy is preserved during the time it takes for that column of gas to disengage. Based on this definition of the constant rate disengagement process, the distance between the bottom of the column and the rear of the small or large bubble swarm would simply be the product of the respective rise velocity and the time elapsed since the initiation of the disengagement process. The analysis presented by Sriram and Mann (1977) assumes a similar disengagement process, the only difference being that they assumed a continuous bubble size distribution.

At any time during the first phase of disengagement (before the large bubbles have left the system), the holdup structure can be represented by Figure 2a. A balance equation for the liquid volume, which remains constant throughout the disengagement process (assuming constant density), can be written as

$$V_\ell = H(t)A_\ell + A_S u_{bS} t + A_L u_{bL} t; \quad t < H_o/u_{bL} \tag{1}$$

Recognizing that before the gas is shut off, holdup fractions for the various components are the same as the area fractions (based on Figure 1) and redefining the liquid volume in terms of the dimensions shown in Figure 1 (i.e., $V_\ell = H_o A_\ell$), Eq. 1 can be modified and rearranged to obtain an expression for dispersion height as

$$H(t) = H_o - \left[\frac{\epsilon_{goL} u_{bL} + \epsilon_{goS} u_{bS}}{1 - \epsilon_{goL} - \epsilon_{goS}}\right] t; \quad t < H_o/u_{bL} \tag{2}$$

A balance equation for the liquid volume, during the second phase of disengagement (Figure 2b) can be written as

$$V_\ell = H(t)(A_\ell + A_L) + A_S u_{bS} t; \quad t \geq H_o/u_{bL} \tag{3}$$

which can also be modified to obtain an expression for dispersion height during the second phase of disengagement

$$H(t) = \frac{H_o(1 - \epsilon_{go})}{1 - \epsilon_{goS}} - \left[\frac{\epsilon_{goS} u_{bS}}{1 - \epsilon_{goS}}\right] t; \quad t \geq H_o/u_{bL} \tag{4}$$

Table 1. Comparison of Approaches*

	Case I (This Work)	Case II (This Work)	Schumpe and Grund (1986)**
Assumption	Constant Disengagement Rate	Interactive Disengagement	Constant Slip Velocity
Average Gas Holdup	$\epsilon_{go} = 1 - \frac{H_s}{H_o}$	$1 - \frac{H_s}{H_o}$	ϵ_{go}
Small Bubble Holdup	$\epsilon_{goS} = 1 - \frac{H_s}{H_o b_2}$	$\frac{s_1 b_2 - s_2}{s_1 - s_2} - \frac{H_s}{H_o}$	$\epsilon_{goS} \cdot \frac{H_2}{H_o}$
Large Bubble Holdup	$\epsilon_{goL} = \frac{H_s}{H_o} \cdot \frac{1 - b_2}{b_2}$	$\frac{s_1(1 - b_2)}{s_1 - s_2}$	$\frac{\epsilon_{goL}}{1 - \epsilon_{goS}}$
Small Bubble Rise Velocity	$u_{bS} = -\frac{H_s s_2}{b_2 - H_s/H_o}$	$H_s s_2 \Big/ \left[\frac{s_1 b_2 - s_2}{s_1 - s_2} - \frac{H_s}{H_o}\right]$	$u_{bS} \cdot \frac{H_s}{H_2}$
Large Bubble Rise Velocity	$u_{bL} = \frac{H_o[s_2 - b_2 s_1]}{1 - b_2}$	$\frac{H_o[s_2 - b_2 s_1]}{1 - b_2}$	$u_{bL} \cdot \frac{u_g - u_{bS}\epsilon_{goS}(H_2/H_o)}{u_g - u_{bS}\epsilon_{goS}(H_o H_s/H_2^2)}$

*Refer to Figure 4 for definitions of heights H_o, H_s and H_2.
**Equations for Schumpe and Grund's approach are given in terms of quantities estimated using case I.

Equations 2 and 4 imply that a plot of dispersion height vs. time is described by two straight lines, one for each phase of disengagement. The equations further show that a plot of dynamic holdup ($\epsilon_g(t) = (H(t) - H_s)/H(t)$) vs. time would yield two straight lines only at very low holdups where an approximation of the dynamic gas holdup ($\epsilon_g(t) \simeq (H(t) - H_s)/H_s$) may be justified.

In Eqs. 2 and 4, the values of steady-state dispersion height (H_o) and gas holdup (ϵ_{go}) can be obtained easily from direct measurements. We are, therefore, left with four unknowns (u_{bL}, u_{bS}, ϵ_{goL}, and ϵ_{goS}). Equations 2 and 4 give four independent expressions relating to these four unknowns, two for the slopes and two for the intercepts of the straight lines. A measurement of the slopes and intercepts from the disengagement profile can now be used to evaluate the holdup fractions and corresponding bubble rise velocities. The expressions for the two holdup fractions and the two rise velocities in terms of the slopes and intercepts, obtained from a plot of normalized height (H/H_o) vs. time, are shown in Table 1. In developing these expressions, we have used a value of 1 for b_1, since the straight line representing the first phase of disengagement intercepts the ordinate at $H/H_o = H_o/H_o = 1$.

The concepts presented above, for the constant rate disengagement process involving a bimodal distribution, are now extended to the case of a multimodal bubble size distribution. For convenience, the disengagement profile can be plotted as normalized height (H/H_o) vs. time and fitted with N straight lines (for a N-bubble class case). The first line represents the first phase of disengagement (largest bubbles leaving the dispersion) and the Nth line represents the last phase (smallest bubbles leaving the system). The slopes (s_i) and intercepts (b_i) for the N lines can be estimated either graphically or by linear regression. It is shown in the Appendix that the resulting generalized expressions for fractional gas holdups and bubble rise velocities are

$$\epsilon_{goi} = \frac{H_s}{H_o}\left[\frac{1}{b_{i+1}} - \frac{1}{b_i}\right]; \quad i = 1 \text{ to } N \tag{5}$$

$$u_{bi} = \frac{H_o[b_i s_{i+1} - b_{i+1} s_i]}{b_i - b_{i+1}}; \quad i = 1 \text{ to } N \tag{6}$$

In the above equations, the $N + 1$th line represents the static liquid height ($b_{N+1} = H_s/H_o$, $s_{N+1} = 0$).

Case II: interactive disengagement process

The disengagement process is defined to be interactive when the disengagement of one class of bubbles affects the disengagement rate of another class. This is likely to happen when there is a significant difference between the total volume of large bubbles and the total volume of small bubbles. During the disengagement of large bubbles, the dispersion level drops rapidly causing a negative liquid flow. This, in turn, hinders the disengagement of small bubbles. The analysis presented here is for the extreme case where no small bubbles leave the system during large bubble disengagement, i.e., the case considered by Vermeer and Krishna (1981). We have further assumed that small bubbles are axially homogeneous following the disengagement of large bubbles. Schumpe and Grund (1986) considered a similar case, where the disengagement of small bubbles was hindered by the large bubbles leaving the system. However, they assumed that the slip velocity for a given bubble class remained constant during the entire disengagement process.

The holdup structure during the first phase of disengagement can be represented by Figure 3a. As the large bubbles leave the system, the liquid level drops and the small bubbles are prevented from disengaging. This results in a net increase in small

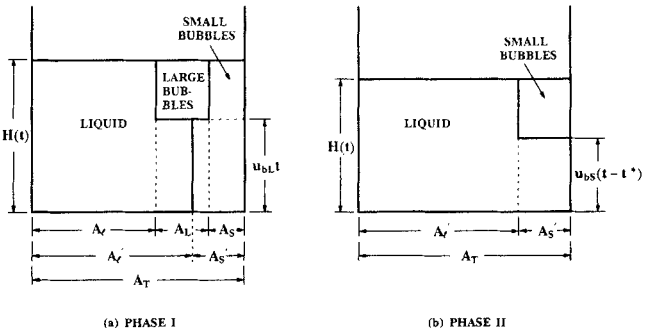

Figure 3. Dispersion during the interactive disengagement process.

bubble holdup in the region between the rear of the large bubble swarm and the bottom of the column. For this case, the combined volume of liquid and small bubbles remains constant, and a volume balance equation can be written as

$$V_\ell + V_S = (A_\ell + A_S)H(t) + A_L u_{bL} t; \quad t < t_1^* \tag{7}$$

where t_1^* is defined by Eq. 9. Equation 7 can be modified and rearranged using geometrical considerations (i.e., $V_\ell = H_o A_\ell$, and $V_S = H_o A_S$), to obtain an expression for dispersion height as

$$H(t) = H_o - \left[\frac{\epsilon_{goL} u_{bL}}{1 - \epsilon_{goL}}\right] t; \quad t < t_1^* \tag{8}$$

At the instant when the rear of the large bubble swarm clears the dispersion, the following must be true.

1. The volume of the dispersion is the combined volume of liquid and small bubbles (which was constant during the first phase).
2. The dispersion height is the product of time elapsed and the rise velocity of large bubbles.

Based on this, an expression for the time (t_1^*), at which small bubbles begin to leave the dispersion, can be written as

$$t_1^* = \frac{(1 - \epsilon_{goL})H_o}{u_{bL}} \tag{9}$$

A schematic of the holdup structure during the second phase of disengagement is shown in Figure 3b. The cross-sectional areas for the liquid and small bubble fractions are related by the respective holdup fractions

$$\frac{A'_\ell}{A'_S} = \frac{1 - \epsilon_{go}}{\epsilon_{goS}} \tag{10}$$

A volume balance equation for the liquid fraction can be written as

$$V_\ell = H(t)A'_\ell + A'_S u_{bS}(t - t_1^*); \quad t \geq t_1^* \tag{11}$$

which can also be modified to obtain an expression for dispersion height during the second phase of disengagement

$$H(t) = H(t_1^*) - \frac{\epsilon_{goS} u_{bS}}{1 - \epsilon_{go}}(t - t_1^*); \quad t \geq t_1^* \tag{12}$$

where $H(t_1^*) = u_{bL} t_1^*$, and t_1^* is defined by Eq. 9. Equations 8 and 12 are linear with respect to time, and it is clear that the disengagement profile under these conditions will also be represented by two straight lines. The expressions for the two holdup fractions and the two rise velocities in terms of the slopes and intercepts, obtained from a plot of normalized height vs. time, are shown in Table 1. The expression for large bubble rise velocity for this case is the same as that obtained for case I (Table 1) as expected, because the assumptions made for case II affect only the disengagement rate of small bubbles.

There is no one set of generalized equations that could be developed to describe interactive disengagement of multimodal distributions, where certain classes of bubbles do not disengage until larger bubbles have left the system. The equations will depend on the particular situation; however, the concepts presented above can easily be extended to any situation.

Comparison of approaches

Having established the theoretical basis for analysis of results from dynamic gas disengagement experiments, we would like to interpret the differences between the various approaches in practical terms, i.e., determine the sensitivity of results to the approach used. The holdup structures obtained from a given disengagement profile, using the different approaches, will be compared. Figure 4 shows a typical disengagement profile (normalized dispersion height vs. time) for a bimodal bubble size distribution. For the constant rate disengagement process (case I), the holdup of small bubbles reduces to

$$\epsilon_{goS} = \frac{H_2 - H_s}{H_2} \tag{13}$$

For case II, where small bubbles disengage only after all of the large bubbles have left the system, the small bubble holdup is

$$\epsilon_{goS} = \frac{H_1 - H_s}{H_o} \tag{14}$$

Schumpe and Grund (1986) have shown that when the analysis is based on constant slip velocity, the normalized height differential ($H_2/H_o - H_s/H_o$) very well approximates the contribution due to small bubbles, and the resulting expression for small bubble holdup is

$$\epsilon_{goS} = \frac{H_2 - H_s}{H_o} \tag{15}$$

It is not possible to present an analytical expression for small bubble holdup based on the constants obtained from a plot of dynamic gas holdup vs. time, because of the inherent approximations involved in fitting such a plot to straight lines, as dis-

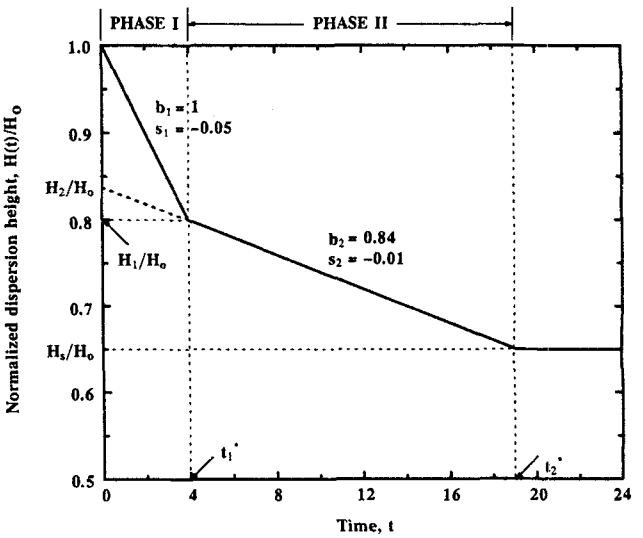

Figure 4. Typical disengagement profile for a bimodal distribution.

cussed earlier. However, it can be shown that the value for small bubble holdup for this case would be very similar to that obtained from Eq. 13. On comparing Eqs. 13, 14 and 15, the following trend is obvious

$$\epsilon_{goS} \text{ (Eq. 13)} > \epsilon_{goS} \text{ (Eq. 15)} > \epsilon_{goS} \text{ (Eq. 14)}$$

and only under the limiting case of no large bubbles, do holdups from the three expressions converge to the same value. In Table 1, we have compared the expressions used to determine holdups and rise velocities for a bimodal distribution, based on cases I and II, and on the approach proposed by Schumpe and Grund (1986). It should be noted that the expressions presented for Schumpe and Grund's approach are somewhat approximate, since the exact values are obtained by an iterative procedure. For the sake of comparison, the equations from the Schumpe and Grund approach are defined in terms of quantities estimated in case I. The dimensions used in these equations refer to those given in Figure 4. It is clear from this table that case I gives higher values for small bubble holdup and small bubble rise velocity, and lower values for large bubble holdup than those obtained from the approach proposed by Schumpe and Grund. Furthermore, it can be shown that, when the contribution to holdup due to small bubbles is low, the large bubble rise velocity from case I will always be lower than that predicted by Schumpe and Grund.

In order to get an appreciation for the magnitude of differences involved in the different approaches, the dimensions shown in Figure 4 are converted to actual distances (assuming that $H_o = 100$ and $H_s = 65$, i.e., a total gas holdup of 35%; and $t_1^* = 4$) and holdup for small bubbles calculated. Equations 13, 14 and 15 gave small bubble holdups of 22.6%, 15%, and 19%, respectively. When the disengagement profile was replotted in terms of dynamic holdup vs. time and a straight line fitted to data from the second phase of disengagement, a value of 24.3% was obtained for small bubble holdup. When the calculations were repeated for different disengagement profiles, it was seen that small bubble holdup obtained using a plot of dynamic holdup vs. time was always higher than values obtained from case I. This analysis shows that great care is necessary while interpreting results from dynamic gas disengagement studies. Furthermore, the approximations involved in using a plot of dynamic holdup vs. time, rather than dispersion height vs. time, increase the error of the technique and should be avoided.

Bubble Rise Velocities. Rise velocities of bubbles in the two classes (for a bimodal distribution) are estimated from the analysis presented above. However, this analysis does not take into account any radial variations in rise velocities due to the presence of circulation patterns. This limitation of the DGD technique has been acknowledged in previous studies (e.g., Sriram and Mann, 1977; Schumpe and Grund, 1986), although no effort has been made to introduce any corrective measures. Visual observations of the dispersion during the disengagement process show that the dispersion is fairly uniform during the second phase of disengagement; however, during the first phase (when large bubbles are still leaving the system) it is possible that strong radial profiles still exist. It is, therefore, expected that the rise velocities of small bubbles, estimated using DGD, are fairly accurate, though this may not be the case for rise velocities of large bubbles.

The small bubble rise velocity obtained from DGD is the swarm rise velocity associated with the class of bubbles disengaging during the second phase. For bubbly flow, typically observed during this phase, the swarm rise velocity is related to the terminal rise velocity of a single bubble in an infinite medium by the relationship proposed by Marrucci (1965).

$$u_{b\infty} = \frac{u_{bS}(1 - \epsilon_{goS}^{5/3})}{(1 - \epsilon_{goS})^2} \tag{16}$$

Equation 16 can be used to estimate the single bubble terminal rise velocity using the small bubble rise velocity and gas holdup values obtained from DGD.

Bubble Size Estimation. The DGD technique gives swarm bubble rise velocities, which are related to terminal rise velocities as described above. Bubble size can be estimated from the knowledge of the terminal rise velocity by using an appropriate correlation. Several correlations are available in literature that relate terminal rise velocity to bubble size (Table 2). The simplest approach would be to use Stokes' law to determine bubble sizes for small bubbles from their terminal rise velocities. However, Stokes' law is limited to situations where $Re < 2$, and could

Table 2. Correlations for Estimating Bubble Size from Bubble Rise Velocity

Reference	Correlation	Range of Applicability
Stokes' Law	$d_{bS} = \left[\frac{18\mu_\ell u_{b\infty}}{g(\rho_\ell - \rho_g)}\right]^{0.5}$	$Re < 2$
Peebles and Garber (1953)	$d_{bS} = 4.76\left[\frac{\mu_\ell}{\rho_\ell}\right]^{0.41} \frac{u_{b\infty}^{0.78}}{g^{0.59}}$	$2 \le Re \le 4.02\left[\frac{g\mu_\ell^4}{\rho_\ell \sigma_\ell^3 g_c^3}\right]^{-0.214}$
Clift et al. (1978)	$u_b = \left[\frac{2.14\sigma_\ell}{\rho_\ell d_b} + 0.505 g d_b\right]^{0.5}$	$d_b > 1.3\ mm$
Abou-el-Hassan (1983)	$V = 0.75[\log(F)]^2$	$710 \le \rho_\ell \le 1{,}180\ \text{kg/m}^3$
	V = velocity number $= \frac{u_b d_b^{2/3} \rho_\ell^{2/3}}{\mu_\ell^{1/3} \sigma_\ell^{1/3}}$	$0.233 \le \mu_\ell \le 59\ \text{mPa} \cdot \text{s}$
		$0.015 \le \sigma_\ell \le 0.072\ \text{N/m}$
		$0.1 \le V \le 40$
	F = flow number $= \frac{g d_b^{8/3}(\rho_\ell - \rho_g)\rho_\ell^{2/3}}{\mu_\ell^{4/3} \sigma_\ell^{1/3}}$	$1 \le F \le 10^6$

not be used in the present study. Therefore, we used the correlations proposed by Abou-el-Hassan (1983) and Peebles and Garber (1953) for small bubbles. The former is a generalized correlation that can be used with a wide variety of liquids and is independent of flow regime, whereas the latter is based on experimental measurements with air bubbles in several liquids including water. For the range of small bubble terminal rise velocities (obtained from Eq. 16) encountered in our studies, it turns out that the two correlations predict similar values for bubble size. The correlation proposed by Clift et al. (1978) was used to estimate large bubble size. This correlation is based on extensive data for bubbles dispersed in water and is valid for bubble sizes greater than 1.3 mm. For lack of a better estimate of the terminal rise velocity for large bubbles, the rise velocity obtained from DGD was used directly in the correlation.

It is important to use the bubble size obtained from this procedure with some caution. In some instances correlations are unable to predict bubble size from known values of rise velocities. This is because the rise velocity remains relatively constant over a wide range of bubble sizes. For example, for tap water the bubble rise velocity is fairly constant for bubbles in the size range 3–10 mm (Clift et al., 1978). A similar problem arises when slug flow is encountered. For a given column diameter, the rise velocity for slugs with different lengths (or different volume-equivalent sphere diameters) is constant. This problem is discussed later in greater detail.

The Sauter mean bubble diameter, which is a volume to surface ratio, is used commonly to determine the specific gas-liquid interfacial area. It is shown in the Appendix that the Sauter mean diameter is given by

$$d_s = \frac{\sum_{i=1}^{N} n_i d_{bi}^3}{\sum_{i=1}^{N} n_i d_{bi}^2} = \frac{\epsilon_{go}}{\sum_{i=1}^{N} \epsilon_{goi}/d_{bi}} \tag{17}$$

The specific gas-liquid interfacial area for the dispersion is then given by

$$a = \frac{6\epsilon_{go}}{d_s} = 6 \sum_{i=1}^{N} \frac{\epsilon_{goi}}{d_{bi}} \tag{18}$$

Discussion of Results

The concepts developed in the previous section are illustrated using results obtained from experiments conducted with the air-tap water system. The shapes of disengagement profiles from experiments made in both the 0.05 m ID and the 0.23 m ID columns indicate the presence of bimodal bubble size distributions in the dispersion, Figure 5. In the analysis presented here, the assumptions made under case I are used to estimate the various parameters. Limited results obtained using case II are presented for the sake of comparison.

Vermeer and Krishna (1981) have shown that the rate at which the dispersion level drops during the first phase of the disengagement process equals the superficial gas velocity in effect just before gas flow was cut off. Schumpe and Grund (1986) have theoretically shown that this must be true. In general, results from our study agree with the premise of the above authors, but they agree better with the data from the large column than from the smaller diameter column. The level in the

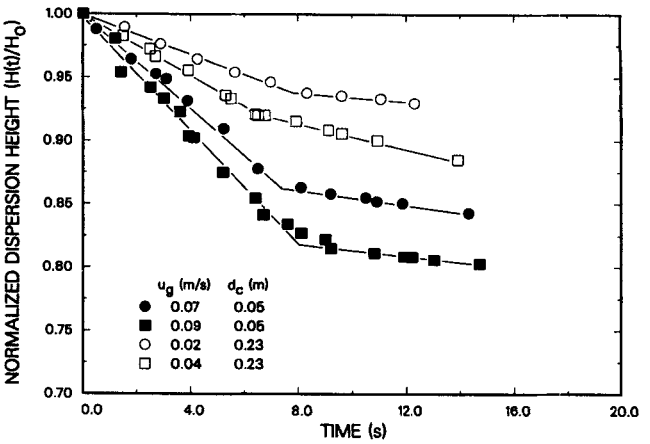

Figure 5. Disengagement profiles at selected gas velocities from experiments with the air-tap water system

Data from runs G2-1 and G9-1

smaller column dropped at a lower rate than expected at higher gas velocities ($u_g > 0.04$ m/s). The major difference between the dispersions in the two columns for this range of gas velocities is in the flow regimes present. The churn-turbulent flow regime is present in the large column, whereas the slug-flow regime is present in the smaller column. It is well known that the terminal rise velocity of a slug is dependent on the column diameter, and it follows that irrespective of the superficial gas velocity, the slug rises at the same velocity once gas flow is terminated. The net result being that the dispersion level drops at a rate which increases only slightly with increasing gas velocity, due to longer and more frequent slugs disengaging from the surface.

Results from a run G2-1 conducted in the 0.05 m ID column, are summarized in Table 3. For each velocity, the size of small bubbles was estimated using the terminal rise velocity for this class of bubbles (Eq. 16). The large bubble rise velocities shown in these tables are those obtained from DGD and from experimental measurements of the time that slugs took to rise between two reference points during the first phase of disengagement. A video camera equipped with an on-screen stopwatch was used to track the slugs. Large bubble rise velocity increased from 0.31 m/s to 0.36 m/s as u_g was increased from 0.01 to 0.04 m/s, thereafter it dropped to 0.28 m/s and did not change when superficial gas velocity was further increased. Visual observations of the dispersion for $u_g \geq 0.04$ m/s showed that the large bubble fraction at these gas velocities consisted mainly of slugs, which coincides with the change in the trend observed for u_{bL} values. The terminal rise velocity for a slug is related to the column diameter by (e.g., Davidson and Harrison, 1963; Clift et al., 1978)

$$u_{b\infty} = 0.35\sqrt{gd_c} \tag{19}$$

Using Eq. 19, the terminal rise velocity of a slug in the 0.05 m ID column is 0.25 m/s, which is in very good agreement with large bubble rise velocities obtained from DGD for $u_g > 0.04$ m/s (Table 3). Slug rise velocities measured with the video camera for $u_g \geq 0.04$ m/s were between 0.28 and 0.32 m/s. These values are in excellent agreement with the value obtained from DGD (0.28 m/s).

Table 3. Results from Run G2-1 (Air-Tap Water System) Conducted in the 0.05 m ID Column*

		Small Bubbles				Large Bubbles					
u_g (m/s)	ϵ_{go}	ϵ_{goS}	u_{bS} (m/s)	$u_{b\infty}$** (m/s)	d_{bS} (mm)	ϵ_{goL}	u_{bL}*** (m/s)	u_{bL}† (m/s)	d_{bL} (mm)	d_s (mm)	a (m^{-1})
0.01	0.026	0.013	0.22	0.23	1.4	0.013	N/A	0.31	18	2.6	60
0.02	0.054	0.024	0.20	0.21	1.3	0.030	N/A	0.33	18	2.7	120
0.03	0.080	0.028	0.21	0.22	1.3	0.052	N/A	0.33	21	3.3	140
0.04	0.100	0.041	0.19	0.21	1.3	0.063	0.28	0.36	50‡	3.2	200
0.05	0.130	0.039	0.18	0.20	1.2	0.087	0.32	0.28	50‡	3.7	210
0.07	0.160	0.046	0.16	0.17	1.1	0.110	0.30	0.28	50‡	3.5	260
0.09	0.190	0.034	0.14	0.15	1.0	0.160	0.30	0.28	50‡	5.2	220

*Analysis based on the constant rate disengagement process approach (case I).
**Terminal rise velocity estimated using Eq. 16.
***Slug rise velocity measured with video camera.
†Large bubble rise velocity from DGD.
‡Equivalent sphere diameter for slug (slug flow).

For a slug whose diameter approaches the column diameter, the diameter of a volume-equivalent sphere is given by

$$d_e = \left[\frac{6V_s}{\pi}\right]^{1/3} = \left[\frac{3d_c^2 h_s}{2}\right]^{1/3} \tag{20}$$

It is evident from Eq. 20 that, for such a slug, the volume-equivalent diameter equals the column diameter when $h_s = 0.67d_c$; furthermore, d_e can be greater than column diameter when $h_s > 0.67d_c$. The slug observed in the 0.05 m ID column had lengths which varied between 0.10 and 0.25 m (i.e., h_s = 2–5 d_c). In Table 3, we have used $d_{bL} = d_e = d_c$, whereas the actual d_{bL} would be greater than d_c if the slug diameter is greater than $0.6d_c$. The latter condition was satisfied in all our experiments with $u_g \geq 0.04$ m/s. For the extreme case, where $h_s = 0.25$ m and slug diameter equals column diameter, Eq. 20 gives $d_e = 98$ mm. When we used this value for the large bubble diameter (i.e., $d_{bL} = d_e = 98$ mm) instead of $d_{bL} = d_c = 50$ mm, the effect on d_s for $u_g \geq 0.04$ m/s was small. The largest change was at $u_g = 0.09$ m/s, where d_s increased by 4% (5.4 vs. 5.2 mm). Therefore, any errors involved in the estimate for large bubble diameter will have little effect on the Sauter mean bubble diameter. This further implies that d_s is strongly influenced by the size and volume fraction of the small bubbles.

Figure 6 compares the average gas hold-up with the contribution due to small bubbles from experiments conducted in the two columns. It is interesting to note that even though average gas holdup profiles are similar for the two columns, the contribution of small bubbles is significantly greater in the large column than in the smaller diameter column. This can once again be attributed to the differences in flow regimes present in the two columns. This observation is similar to the findings of Schumpe and Grund, who conducted experiments in the heterogeneous flow regime (churn-turbulent flow regime) in a 0.3 m ID column, and results obtained by Godbole et al. (1982) for the air-water system in a 0.1 m ID column. In both of these studies, the churn-turbulent flow regime favored a higher contribution to holdup by small bubbles. The small bubble holdup (Figure 6) for $u_g \geq 0.04$ m/s is either constant (0.05 m ID column) or increases slightly (0.23 m ID column), whereas the holdup due to large bubbles increases steadily with gas velocity, Tables 3 and 4.

The small bubble rise velocities in both columns (Tables 3 and 4) are similar and remain fairly constant over the range of superficial gas velocities employed. In contrast, large bubble rise velocities for the two columns differ significantly. They are significantly higher in the large column than in the smaller diameter column, due to the presence of slugs in the small column with a constant rise velocity. A direct quantitative comparison of these values with those obtained by Schumpe and Grund is not possible because of the differences in rise velocity definitions for the two situations. However, their results agree qualitatively with those from the present study. They also found that the small bubble rise velocity remained fairly constant, whereas the rise velocity of large bubbles increased significantly with an increase in superficial gas velocity. The values for large bubble rise velocity from their study are significantly greater than those from our study, which is expected based on our previous discussion (Table 1).

Figure 7 compares the Sauter mean diameters obtained from measurements made in the two columns. As expected, the Sauter mean diameters for the large column are lower than those for the small column for $u_g > 0.03$ m/s, because holdup in the large column is primarily due to small bubbles (churn-turbulent flow regime), while slugs contributed greatly to the holdup in the small column. At low gas velocities ($u_g \leq 0.03$ m/s), however, similar values for d_s are obtained in the two columns. For this range of gas velocities, both columns are expected to operate in the homogeneous bubbly flow regime

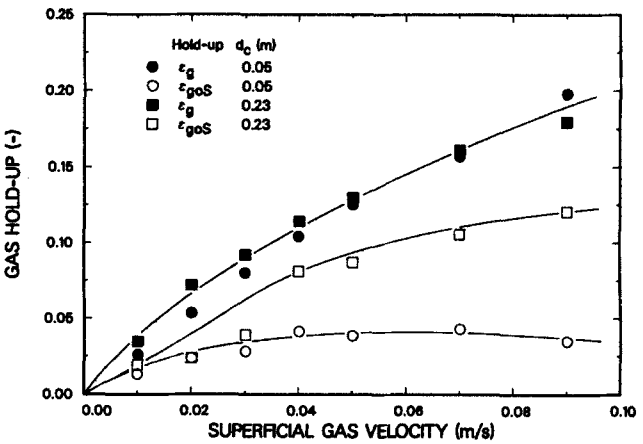

Figure 6. Effect of column diameter and contribution of small bubbles to total gas hold-up.
Analysis based on Case I; Data from Runs G2-1 and G9-1

Table 4. Results from Run G9-1 (Air-Tap Water System) Conducted in the 0.23 m ID Column*

		Small Bubbles				Large Bubbles				
u_g (m/s)	ϵ_{go}	ϵ_{goS}	u_{bS} (m/s)	$u_{b\infty}$** (m/s)	d_{bS} (mm)	ϵ_{goL}	u_{bL} (m/s)	d_{bL} (mm)	d_s (mm)	a (m^{-1})
0.01	0.035	0.019	0.21	0.22	1.3	0.016	0.39	30	2.3	91
0.02	0.072	0.024	0.19	0.19	1.2	0.048	0.25	9	2.8	150
0.03	0.092	0.039	0.18	0.20	1.2	0.053	0.30	16	2.6	220
0.04	0.110	0.081	0.14	0.16	1.0	0.033	0.42	35	1.4	490
0.05	0.130	0.087	0.19	0.23	1.3	0.043	0.44	39	1.9	410
0.07	0.160	0.110	0.18	0.22	1.3	0.052	0.50	50	1.9	510
0.09	0.180	0.120	0.18	0.22	1.3	0.059	0.89	160	1.9	560

*Analysis based on the constant rate disengagement process approach (case I).
**Terminal rise velocity estimated using Eq. 16.

with similar bubble size distributions. Two additional experiments were conducted, one in each column, to check for reproducibility of results. Sauter mean diameters obtained from these repeat runs are also included in Figure 7. Results from these two sets of experiments are in very good agreement with each other. The largest deviation occurred at $u_g = 0.09$ m/s in the 0.05 m ID column, where d_s values from the two runs were 4 and 5 mm, respectively.

The d_s values for the 0.05 m ID column (2–5 mm) are lower than those obtained by Sada et al. (1987) in a 0.078 m ID column (5–9 mm). They calculated d_s values from holdup values and specific gas-liquid interfacial areas obtained using the sulfite oxidation method. Akita and Yoshida (1974) reported Sauter mean diameters in the range 3–5 mm from photographic measurements made during experiments conducted in a 0.15 m ID column equipped with 0.4 mm perforated-plate distributors. In all studies referenced here, d_s values were independent of gas velocity. In general, Sauter mean diameters reported in literature are somewhat higher than those obtained in our study using DGD data and assumptions made under case I. In Table 5, d_s values obtained using assumptions made under case II are compared with those obtained using case I. Significantly higher values are obtained using case II (8–13 mm) compared to those obtained using case I (2–5 mm) for the 0.05 m ID column. The differences in Sauter mean diameters and gas-liquid interfacial areas arising from the use of different assumptions in the data reduction procedure were smaller for experiments conducted in the 0.23 m ID column. These results show that Sauter mean bubble diameter values reported in literature are lower than those obtained using case II and higher than those obtained using case I.

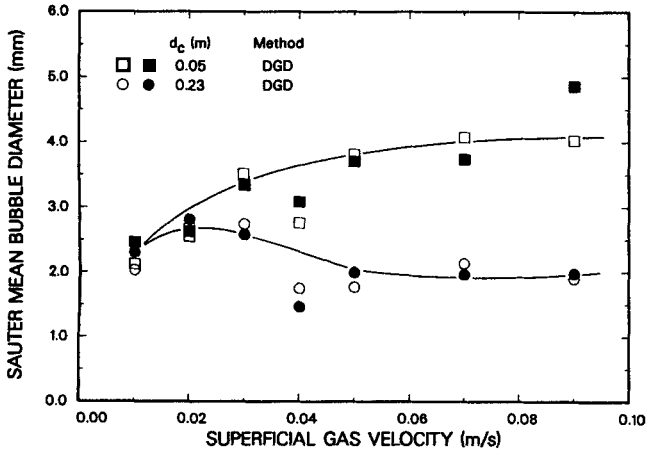

Figure 7. Effect of column diameter on the Sauter mean bubble diameter and reproducibility of results.
Analysis based on Case I; ■—Run G2-1; □—Run G2-2; ●—Run G9-1; O—Run G9-2

The specific gas-liquid interfacial areas for the air-tap water system from two sets of runs are shown in Figure 8. The areas are significantly higher for the large column than those for the small column, due to the larger fraction of small bubbles in the 0.23 m ID column. Reproducibility of results for interfacial areas is very good for both columns. The largest deviation between two runs occurred at $u_g = 0.04$ m/s in the 0.23 m ID column (370 vs. 480 m^{-1}).

Schumpe and Deckwer (1982) used the sulfite oxidation technique to estimate specific gas-liquid interfacial areas and have presented results for the air-water system in a 0.14 m ID bubble column equipped with a 1 mm perforated plate distributor. They showed that the specific area increased with gas velocity and reached 150 m^{-1} at a gas velocity of 0.05 m/s. They also observed slug flow in their column and it appears that conditions were similar to those encountered in the 0.05 m ID column in our work. Figure 8 shows a specific area of 200 m^{-1} in this column at a gas velocity of 0.05 m/s, which is in fairly good agreement with their results. Sada et al. (1987) found similar values when the same technique was used in their 0.078 m ID column. Specific areas approached 200 m^{-1} as gas velocity approached

Table 5. Comparison of Sauter Mean Bubble Diameters and Specific Interfacial Areas Obtained from the Two Cases*

	0.05 m ID Column (Run G2-1)				0.23 m ID Column (Run G9-1)			
	Case I		Case II		Case I		Case II	
u_g (m/s)	d_s (mm)	a (m^{-1})	d_s (mm)	a (m^{-1})	d_s (mm)	a (m^{-1})	d_s (mm)	a (m^{-1})
0.01	2.5	63	9.0	17	2.3	91	7.0	30
0.02	2.6	120	10.0	32	2.8	150	6.6	66
0.03	3.3	140	8.4	58	2.6	220	7.2	77
0.04	3.1	200	8.2	77	1.5	470	4.2	170
0.05	3.7	200	9.0	84	2.0	390	4.2	180
0.07	3.7	250	13.0	73	2.0	490	3.4	290
0.09	4.9	240	10.0	110	2.0	550	2.9	380

*Case I, constant rate disengagement process; case II, interactive disengagement process.

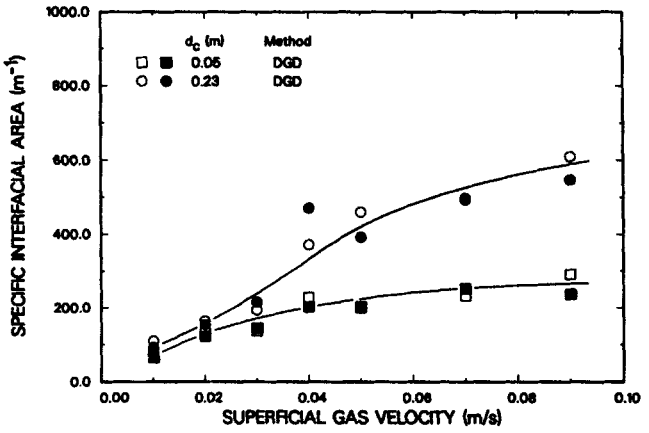

Figure 8. Effect of column diameter on the specific gas-liquid interfacial area and reproducibility of results.

Analysis based on Case I; ■—Run G2-1; □—Run G2-2; ●—Run G9-1; ○—Run G9-2

0.10 m/s in their study, which is in excellent agreement with the results for the 0.05 m ID column shown in Figure 8. Towell et al. (1965) report areas in the range 50–200 m^{-1} for gas velocities in the range 0.01–0.13 m/s in a 0.41 m ID column using the photographic technique. These values are significantly lower than the values obtained from the present study in the 0.23 m ID column (100–600 m^{-1}), for assumptions made under case I. When assumptions made under case II were used to estimate specific gas-liquid interfacial areas, significantly lower values (30–380 m^{-1}) were obtained (Table 5). These values are in better agreement with results of Towell et al. It is also possible that some of the discrepancies between the results from the various studies may be due to the differences in the quality of the tap water used (different concentrations of surfactants, etc.).

We have successfully employed the DGD technique to characterize hydrodynamics of several other systems including pure *n*-butanol, and aqueous solutions of *n*-butanol or *n*-butanol and carboxymethyl celluose (Bukur et al., 1988). Results from studies with molten waxes as the liquid medium at high temperatures have been reported by Bukur et al. (1986, 1987a, b). This system is of interest in the design of bubble column reactors for indirect coal liquefaction via Fischer-Tropsch synthesis. Results from multiple runs with the nitrogen-molten wax system showed excellent reproducibility for Sauter mean bubble diameters. Also, these results compared favorably with d_s values obtained using the photographic technique (Bukur et al., 1986, 1987a).

Conclusions

The main advantage of the dynamic disengagement technique lies in its simplicity and its ability to provide a wide range of information about bubble column hydrodynamics. Because of this, it has found widespread use in recent years. We have presented the various approaches that could be used to analyze the disengagement profile and obtain the holdup structure, bubble sizes, Sauter mean bubble diameters, and gas-liquid interfacial areas. We have also shown that the common practice of using the dynamic gas holdup vs. time plot to estimate the holdup structure increases the error of the technique and should be avoided. Also, we have presented a generalized procedure that can be used to analyze data from a dispersion containing a multimodal bubble size distribution.

Results from experiments conducted with the air-tap water system in 0.05 and 0.23 m ID columns were used to illustrate the application of the technique. Results obtained from experiments conducted in the 0.05 m ID column using case I (constant rate disengagement process) are in good agreement with literature data obtained using conventional techniques for bubble size and specific gas-liquid interfacial area measurements. When the technique was applied to disengagement profiles from the 0.23 m ID column, Sauter mean bubble diameters were lower than those presented in literature. Better agreement was obtained when case II (interactive disengagement process) was used to analyze our data. On the basis of results for the air-tap water system, it appears that these two approaches for data analysis (cases I and II) provide the upper and lower brackets for the Sauter mean bubble diameter and the specific gas-liquid interfacial area. Also, the DGD technique was able to discern between the flow regimes in the two columns, correctly indicating a larger contribution to holdup by smaller bubbles in the 0.23 m ID column than in the 0.05 m ID column.

The dynamic gas disengagement technique has some limitations resulting from the assumptions made, deficiencies in the data collection/analysis procedures, and from its dependence on correlations relating terminal bubble rise velocity to bubble size. The assumption of no bubble-bubble interaction might cause inaccuracies in results for systems with high coalescence rates. Furthermore, the accuracy of Sauter mean diameter estimates for a given system is dependent upon the availability of accurate correlations relating bubble sizes to bubble rise velocities in that system. However, in spite of these limitations, the dynamic gas disengagement technique in its present form gave good results with several systems studied.

Acknowledgment

This work was supported in part by U.S. Department of Energy under contract DE-AC22-84PC70027 and by Center for Energy and Mineral Resources at Texas A&M University.

Notation

a = specific gas-liquid interfacial area, m^{-1}
A, A' = cross-sectional area associated with liquid or with a bubble class, m^2
A_T = cross-sectional area of the bubble column, m^2
b_i = intercept associated with the ith line
d_b = bubble diameter, mm
d_{bi} = diameter of a bubble in the ith class, mm
d_c = column diameter, m
d_e = diameter of a volume equivalent sphere, mm
d_s = Sauter mean bubble diameter, mm
F = flow number
g = acceleration due to gravity, m/s^2
g_c = gravitational constant, Nm^2/kg^2
h_s = slug length, m
H = dispersion height, m
H_s = static or ungassed liquid height, m
n_i = number of bubbles in class i
Re = Reynolds number, $d_{bS}u_{b\infty}\rho_L/\mu_L$
s_i = slope associated with the ith line, s^{-1}
t = time, s
t_i^* = time marking the end of the ith phase of disengagement, s
u_b = bubble rise velocity, m/s
u_{bi} = rise velocity for bubbles in the ith class, m/s
$u_{b\infty}$ = terminal rise velocity of a single bubble or slug, m/s
u_g = superficial gas velocity, m/s
V = velocity number, volume

V_i = volume of a single bubble in the ith class, mm^3
V_s = volume of a slug, m^3
V_T = total volume of the dispersion, m^3

Greek letters

$\epsilon_g(t)$ = dynamic gas holdup
ϵ_{go} = average gas holdup
ϵ_{goi} = holdup associated with bubbles in the ith class
μ = viscosity, mPa · s
ρ = density, kg/m^3
σ = surface tension, N/m

Subscripts

1 = first phase of disengagement
2 = second phase of disengagement
b = bubble
g = gas
ℓ = liquid
L = large bubbles
o = at time $t = 0$
S = small bubbles

Literature Cited

Abou-el-Hassan, M. E., "A Generalized Bubble Rise Velocity Correlation," *Chem. Eng. Commun.*, **22**, 243 (1983).

Akita, K., and F. Yoshida, "Bubble Size, Interfacial Area, and Liquid-Phase Mass Transfer in Bubble Columns," *Ind. Eng. Chem. Process Des. Dev.*, **13**, 84 (1974).

Bukur, D. B., J. G. Daly, S. A. Patel, R. Matheo, and G. B. Tatterson, "Hydrodynamic Parameters for the Fischer-Tropsch Synthesis in Bubble Column Reactors," *Proc. DOE Indirect Liquefaction Contractors' Mtg.*, Monroeville, PA, 126 (Dec. 3–4, 1986).

Bukur, D. B., J. G. Daly, S. A. Patel, M. L. Raphael, and G. B. Tatterson, "Hydrodynamics of Fischer-Tropsch Synthesis in Slurry Bubble Column Reactors," Final Report to the Dept. of Energy for Contract DE-AC22-84PC70027 (1987a).

Bukur, D. B., S. A. Patel, and R. Matheo, "Hydrodynamic Studies in Fischer-Tropsch Derived Waxes in a Bubble Column," *Chem. Eng. Commun.*, **60**, 63 (1987b).

Bukur, D. B., and S. A. Patel, "Hydrodynamic Studies with Foaming and Non-Newtonian Solutions in Bubble Columns," *Can. J. Chem. Eng.*, submitted (1988).

Clift, R., J. R. Grace, and M. E. Weber, *Bubble Drops and Particles*, Academic Press, New York, 171, 236 (1978).

Davidson, J. F., and D. Harrison, *Fluidised Particles*, Cambridge University Press, U.K., 21 (1963).

Godbole, S. P., M. F. Honath, and Y. T. Shah, "Holdup Structure in Highly Viscous Newtonian and non-Newtonian Liquids in Bubble Columns," *Chem. Eng. Commun.*, **16**, 119 (1982).

Godbole, S. P., A. Schumpe, Y. T. Shah, and N. L. Carr, "Hydrodyanmics and Mass Transfer in non-Newtonian Solutions in a Bubble Column," *AIChE J.*, **30**, 213 (1984).

Kelkar, B. G., S. P. Godbole, M. F. Honath, Y. T. Shah, N. L. Carr, and W. D. Deckwer, "Effect of Addition of Alcohols on Gas Holdup and Backmixing in Bubble Columns," *AIChE J.*, **29**, 361 (1983).

Kuo, J. C. W., "Two-Stage Process for Conversion of Synthesis Gas to High Quality Transportation Fuels," Final Report to the Dept. of Energy for Contract DE-AC22-83PC60019 (1985).

Lee, Y. H., Y. J. Kim, B. G. Kelkar, and C. B. Weinberger, "A Simple Digital Sensor for Dynamic Gas Holdup Measurements in Bubble Columns," *Ind. Eng. Chem. Fund.*, **24**, 105 (1985).

Marrucci, G., "Rising Velocity of a Swarm of Spherical Bubbles," *Ind. Eng. Chem. Fund.*, **4**, 224 (1965).

Peebles, F. N., and H. J. Garber, "Studies on the Motion of Gas Bubbles in Liquids," *Chem. Eng. Prog.*, **49**, 88 (1953).

Sada, E., H. Kumazawa, C. H. Lee, and H. Narukawa, "Gas-Liquid Interfacial Area and Liquid-Side Mass-Transfer Coefficient in a Slurry Bubble Column," *Ind. Eng. Chem. Res.*, **26**, 112 (1987).

Schumpe, A., and W. D. Deckwer, "Gas Holdups, Specific Interfacial Areas, and Mass Transfer Coefficients of Aerated Carboxymethyl Cellulose Solutions in a Bubble Column," *Ind. Eng. Chem. Process Des. Dev.*, **21**, 706 (1982).

Schumpe, A., and A. Grund, "The Gas Disengagement Technique for Studying Gas Holdup Structure in Bubble Columns," *Can. J. Chem. Eng.*, **64**, 891 (1986).

Sriram, K., and R. Mann, "Dynamic Gas Disengagement: a New Technique for Assessing the Behavior of Bubble Columns," *Chem. Eng. Sci.*, **32**, 571 (1977).

Towell, G. D., C. P. Strand, and G. H. Ackerman, "Mixing and Mass Transfer in Large Diameter Bubble Columns," *AIChE–Inst. Chem. Eng. Symp. Ser.*, No. 10 (1965).

Vermeer, D. J., and R. Krishna, "Hydrodynamics and Mass Transfer in Bubble Columns Operating in the Churn-Turbulent Regime," *Ind. Eng. Chem. Process Des. Dev.*, **20**, 475 (1981).

Weimer, A. W., D. C. Gyure, and D. E. Clough, "Application of a Gamma-Radiation Density Gauge for Determining Hydrodynamic Properties of Fluidized Beds," *Powder Technol.*, **44**, 179 (1985).

Appendix

Development of generalized equations for case I

The generalized equations for estimating fractional gas holdups and bubble rise velocities for the various bubble sizes in a multimodal bubble size distribution (N bubble classes) are derived here. The derivations are for the constant rate disengagement process (case I). We can partition the dispersion into $N + 1$ fractions (liquid fraction, and N gas fractions for the N bubble classes) similar to what we had done in Figure 1 for the bimodal distribution.

At any instant during the disengagement process, the balance equation for the liquid volume (which is always constant) can be written as

$$V_\ell = H(t)A_\ell + H(t)\sum_{i=1}^{k-1} A_i + t\sum_{i=k}^{N} A_i u_{bi} \qquad \text{(A1)}$$

The first term on the righthand side represents the volume of liquid that still remains in the section originally occupied by the entire liquid fraction, the second term represents the volume displaced due to the complete disengagement of the first $(k-1)$ bubble classes, and the last term represents the volume displaced due to the partial disengagement of the remaining $(N-k+1)$ bubble classes. Recalling that area fractions are the same as the holdup fractions and using the equality $(V_\ell = H_o A_\ell)$, Eq. A1 yields, upon rearrangement

$$\frac{H(t)}{H_o} = \frac{H_s/H_o}{1-\sum_{i=k}^{N}\epsilon_{goi}} - t\,\frac{\sum_{i=k}^{N}\epsilon_{goi}u_{bi}}{H_o\left[1-\sum_{i=k}^{N}\epsilon_{goi}\right]} \qquad \text{(A2)}$$

This is an equation of a straight line describing the disengagement profile during the kth phase of disengagement, with an intercept of

$$b_k = \frac{H_s/H_o}{1-\sum_{i=k}^{N}\epsilon_{goi}} \qquad \text{(A3)}$$

and a slope of

$$s_k = -\frac{\sum_{i=k}^{N}\epsilon_{goi}u_{bi}}{H_o\left[1-\sum_{i=k}^{N}\epsilon_{goi}\right]} \qquad \text{(A4)}$$

Equation A3 can be rearranged to give the fractional gas holdup corresponding to the kth bubble class

$$\epsilon_{gok} = 1 - \frac{H_s}{H_o b_k} - \sum_{i=k+1}^{N} \epsilon_{goi} \tag{A5}$$

The expression for the intercept of the straight line representing the $k + 1$th phase of disengagement can be manipulated to give

$$\sum_{i=k+1}^{N} \epsilon_{goi} = 1 - \frac{H_s}{H_o b_{k+1}} \tag{A6}$$

Combining Eqs. A5 and A6 we get an expression for the fractional gas holdup for the kth bubble class in terms of measured quantities

$$\epsilon_{gok} = \frac{H_s}{H_o}\left[\frac{1}{b_{k+1}} - \frac{1}{b_k}\right] \tag{A7}$$

Expressions for the intercept and slope (Eqs. A3 and A4) can be combined to get

$$\sum_{i=k}^{N} \epsilon_{goi} u_{bi} = -\frac{s_k H_s}{b_k} \tag{A8}$$

which upon further manipulation gives the expression for the rise velocity of bubbles belonging to the kth class

$$u_{bk} = \left[-\frac{s_k H_s}{b_k} - \sum_{i=k+1}^{N} \epsilon_{goi} u_{bi}\right]\frac{1}{\epsilon_{gok}} \tag{A9}$$

Combining expressions for the intercept and slope of the line representing the $k + 1$th phase of disengagement yields

$$\sum_{i=k+1}^{N} \epsilon_{goi} u_{bi} = -\frac{s_{k+1} H_s}{b_{k+1}} \tag{A10}$$

Combining Eqs. A7, A9 and A10 we get an expression for the rise velocity of bubbles belonging to the kth class

$$u_{bk} = \frac{H_o[b_k s_{k+1} - b_{k+1} s_k]}{b_k - b_{k+1}} \tag{A11}$$

We can now present the general expressions for fractional holdups and rise velocities in terms of intercepts and slopes of straight line segments used to describe the disengagement profile. The intercepts and slopes are obtained from a plot of normalized dispersion height ($H(t)/H_o$) vs. time.

$$\epsilon_{goi} = \frac{H_s}{H_o}\left[\frac{1}{b_{i+1}} - \frac{1}{b_i}\right]; \quad i = 1 \text{ to } N \tag{A12}$$

$$u_{bi} = \frac{H_o[b_i s_{i+1} - b_{i+1} s_i]}{b_i - b_{i+1}}; \quad i = 1 \text{ to } N \tag{A13}$$

Development of the expression for Sauter mean bubble diameter

The definition of the Sauter mean bubble diameter assumes spherical bubbles and is given by

$$d_s = \frac{\sum_{i=1}^{N} n_i d_{bi}^3}{\sum_{i=1}^{N} n_i d_{bi}^2} \tag{A14}$$

The number of bubbles (n_i) of size d_{bi} can be estimated as follows. The overall average gas holdup can be defined by

$$\epsilon_{go} = \sum_{i=1}^{N} \epsilon_{goi} = \frac{\sum_{i=1}^{N} n_i V_i}{V_T} \tag{A15}$$

Therefore, the number of bubbles in a given bubble class can be written as

$$n_i = \frac{\epsilon_{goi} V_T}{V_i} \tag{A16}$$

Recognizing that the volume of an individual bubble is $\pi d_{bi}^3/6$ and the total volume of the dispersion is $\pi d_c^2 H_o/4$, Eq. A16 can be rewritten as

$$n_i = \frac{3\epsilon_{goi} d_c^2 H_o}{2 d_{bi}^3} \tag{A17}$$

Substituting the expression for n_i from Eq. A17 into the definition of the Sauter mean bubble diameter (Eq. A14) we get, upon rearrangement

$$d_s = \frac{\epsilon_{go}}{\sum_{i=1}^{N} \epsilon_{goi}/d_{bi}} \tag{A18}$$

Manuscript received Dec. 5, 1988, and revision received Feb. 21, 1989.